Probing pores by stars – An essential module in a porosimetry and permeability estimation methodology of virtual cement paste

Piet Stroeven

Faculty of Civil Engineering and Geosciences, Delft University of Technology, Stevinweg 1, 2628 CN Delft, the Netherlands

Experimental approaches to permeability assessment are time-consuming and as a consequence expensive. A virtual methodology has therefore been developed that is more economical. Herein, reliability can be guaranteed by unbiased data extraction from the simulated cementitious materials that are of a sufficiently realistic nature. Unfortunately, proper validation of the virtual approach cannot readily be accomplished due to recognized shortcomings of the common experimental approach. To achieve a realistic fresh cement particles dispersion, the discrete element method (DEM) is employed, instead of the in concrete technology popular random sequential addition (RSA) approach. This has direct impact on the pore depercolation process during hydration simulation, and thus on the final outcomes of porosimetry. The unbiased measuring of pore size in the resulting very complex capillary pore network structure is the topic covered in this paper. It is a crucial module in the relevant sequence of modules building up the full methodology. "Probing pores by stars" has probably its roots in spatial statistics. Although unknown in concrete technology, a star volume measuring (SVM) method is employed in experimental life science research and used as starting point for further developments. A brief sketch is presented of the various modules to inform the readers about the full potential of the methodology that ultimately offers estimates on permeability. A short discussion is finally provided on the different methodological routes for permeability estimation on the basis of porosimetry data obtained by probing pores by stars.

Key words: Particle packing, virtual cement, porosimetry, star probing, robotics, permeability, SVM

1 Introduction

Capillary pores play an important role in concrete because they can transport water and other harmful substances through the concrete body. This may lead to deterioration of the concrete or the steel reinforcement and will thus ultimately cause durability problems. Detection of such pores to estimate their sizes has therefore been the subject of many studies in concrete technology. Popular methods to do so involve 3D approaches by Mercury Intrusion Porosimetry (MIP) and Wood's Metal Intrusion Porosimetry (WMIP). These test are straight-forward, but the evaluation of the geometric pore characteristics requires significant and in fact unrealistic schematization of the pore network structure. The deficiencies of such methods for tackling the problem have been explicitly described in the literature [1-5]. WMIP has the advantage over MIP that Wood's Metal solidifies, so that sections of the concrete specimen can be independently investigated. This leads to the second popular way of studying pores in concrete, i.e., by quantitative image analysis. Mostly the approach is of two-dimensional (2D) character, although stereological tools would allow for 3D interpretation [6-15]. Of course, the latter puts a strong impetus on the sampling strategy, which makes the approach more complicated and time-consuming. Nevertheless, this paper will present some stereological notions that render possible defining in this 3D setting, among other things, pore size as targeted in this paper.

Due to progress in computer technology, researchers are nowadays tempted to produce concrete in virtual reality. Two approaches are popular in concrete technology, *i.e.* random sequential addition (RSA) [15-21] and the discrete element method (DEM). DEM with a dynamic stage for simulating particle interferences at increasing packing density can be considered superior, since the production conditions of the material are also simulated. RSA leads to too evenly distributed particles, because of the absence of particle interferences. Properties that are depending on details of the particle dispersion (so called structure-sensitive properties) will therefore be obtained in a biased way [4, 5, 23-28]. DEM is thus more versatile and should be preferred, unless the property at issue can be proven structure-insensitive, indeed. For more DEM systems, see [29-39]. Particularly [39] has a more general scope where it surveys methods producing "a distributed discrete element modelling environment". Not a single RSA approach is mentioned.

Laborious investigations can be readily executed in virtual reality. Such a method is serial sectioning and 3D reconstruction [40]. The pore network that results from the simulated

hydration process is sampled in this publication by sections that are so closely spaced that (dis)continuity in the network structure can be investigated. Far simpler, novel methods are based on random-walk related algorithms developed in robotics [41-46]. Basically, network structures (so called "trees") are formed of unobstructed straight lines connecting neighbouring points inside pore space. This principle has been explored in our DRaMuTS module, as introduced in section 4.2. The pore "channels" that connect outer sides of the specimen can be distinguished from dead-end pores branching off such channels and from fully isolated pores. So, pore topology can directly be assessed.

The pore structure in the hydrated virtual cement as assessed by DRaMuTS is complex, revealing irregularly-shaped pore channels that form a tortuous and partly connected network. This leaves the relevant question of how to determine pore size in an optimum way in such a complicated situation. Optimization in facing this problem involves profiting from relevant, reliable developments exploited elsewhere and accounting for the economy of the developed approach in laying down a practical implementation of the methodology in a new module. Hereby we should acknowledge, of course, that size and shape are interrelated geometric characteristics [47-52]. So, an unambiguous response to the posed question would be impossible. Hence, an arbitrary element in its assessment cannot be avoided, despite pore size being commonly accepted as a leading parameter in durability issues. This will be touched upon in a separate section.

The major conclusion drawn from the available literature (also listed in this paper) is that star volume measuring (SVM), used in experimental settings in life sciences, would be the best starting point, since offering potentially an optimum solution to demands for reliability and economy. Note that SVM estimates the volume of the representative sphere on the basis of measurements in the (2D) section plane revealing irregularly shaped pore sections; modern stereology *pur sang*. Hence, our research goal was emphasized as transforming SVM into a basically 3D approach founded on the same reliable stereological basis. Supposedly, 3D stars situated inside pore space could be employed to measure pore size (in terms of the diameter of the representative sphere). This concept should be provided with a geometrical statistical (=stereological) basis. Further, the implementations into a practical and economic methodology formed also part of the research goal.

2 Size and shape

Let us first face the type of problems that one can expect in surveying simple examples as indicated in Figure 1.

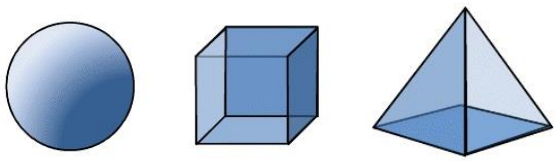

Figure 1. Simple, differently-shaped 3D elements (sphere, cube and pyramid)

The simplest case is that of a spherical particle. Size is unambiguously defined by the sphere's diameter. The cube already leads to problems with size definition. Different lineal size parameters can be associated with the length of rib, face diagonal or space diagonal (in proportions 1: $\sqrt{2}$: $\sqrt{3}$). Common size measures are further the diameter of the inscribed and circumscribed spheres, coinciding for the cube with the length of the rib and of the space diagonal, respectively. Another linear size measure is the diameter of the sphere with identical volume (= $\sqrt[3]{6/\pi}$ = 1.46), the so-called average or representative sphere. So, even for single particles, size cannot be unambiguously defined; it needs for its assessment a definition, which should be functional to the engineering problem faced.

Finally, the size of the pyramid could be associated with its rib length. Alternatively, the bottom face diagonal is longer ($\sqrt{2}$), and can also be employed. Doubling the pyramid by adding two at the bottom face will double its volume, but not necessarily influence the size measures because rib length is identical and the height of the double pyramid as largest dimension is $\sqrt{2}$. The diameter of the representative sphere of a single pyramid is 0.77 times its rib length.

So, it can be concluded that with equal volume of the particles in Figure 1 and thus of the representative spheres, the linear size measures of the particles will be quite different. As a consequence, *the shape of the object influences the size of the representative sphere at equal size of the objects*. This is a relevant conclusion when using the representative sphere concept for modelling and size probing of the pores in the network structure.

For another engineering problem, relevant for concrete technology, *i.e.*, sieving of aggregate, we have to face irregularly shaped particles. Ellipsoidal shape has been demonstrated functional for river gravel particles in virtual materials, and polyhedra shape for crushed rock aggregate particles. In this case, the size of the representative sphere is not a proper measure for size probing by the sieve. In general, passage through the sieve will be associated with a lineal particle measure *somewhere* in between extremes, such as the diameters of the inscribed and circumscribed spheres, depending on the energy regime. The result depends also on actual shape of the particles, of course. It is not surprising therefore that the sieve curve offers a biased representation of the particle size distribution function, as shown already long ago by Vieser [52, 53]. This process could be simulated eventually by the present DEM system.

When isolated (*e.g.*, air entrained) pores are emphasized as spherical, the section pattern will reveal circular pore sections (diameter x). It is well-known that the size distribution of the circles in the section plane cannot be directly correlated with the size distribution of the spheres. This problem persists when we deal with mono-size spheres with diameter D_0.

The literature just provides a way to correlate the moments of both distribution functions [54]. For the average pore circle size this yields for the simplest, mono-size, case

$$\bar{x} = \frac{\pi}{4} D_0 \tag{1}$$

Hence, average 2D pore size significantly underscores its 3D equivalent.

So called "enveloping" techniques were originally developed for the required cumbersome numerical procedures in the general case of multi-size spheres in 3D and a multi-size 2D section size distribution available in experimental settings [6, 15]. Nowadays, SVM would be the proper approach: a modern (non-traditional) stereological method.

When the actual tree structure of capillary pores would be replaced by all representative spheres in the dispersed points, the resulting structure of intersecting spheres would be a transformation of the actual structure with *identical size but modified shape*. Of course, application for permeability assessment will require determination of all intersection circles as *throats* that primarily govern transport of water through the system. This can be

done. However this is not the way probing pores by stars is realized in the methodology designed for permeability estimation. We will discuss our more direct approach later.

Obviously, the hydration of binder particles gradually causes a reduction in free space. As a result of this pore de-percolation process, a complex and partly connected network structure of pores is resulting [55, 56]. Hence, pores will be tortuous, branching and will have irregularly-shaped cross sections. This raises the relevant question as to how size in the context of such a puzzling variety of shapes should be *defined*. As stated earlier, the representative circle and sphere concepts are most appropriate in defining local size of the pores, while probing by stars will be demonstrated a straight forward, reliable and economic way in assessment of the sizes of such representative circles and spheres. However, first of all, the spatial pore network structure should be visualized or made accessible. Complete visualization of the network in physical experiments would be quite impossible. Nevertheless, options could be explored in virtual reality, as was demonstrated.

3 Size characterization in 3D

Three methods would be readily available for 3D assessment of pore size distribution based on 2D sections in physical experiments. Successively, stereological methods, the mathematical morphology operator "opening" and the star volume observation technique can be mentioned. Specific interpretations of "size" are involved in the different approaches. In virtual reality, the latter two methods can potentially be applied in 3D. The opening operation is performed in 2D on a digitized image of the section pattern and should be similarly applied on a digitized virtual structure. This are not the conditions offered by our DEM approach, however.

*3.1 **Stereological methods***

Stereology encompasses geometrical statistical tools providing means for unbiased estimation of 3D geometrical parameters of the state of aggregation in materials on the basis of one-dimensional (1D) or 2D observations [6, 13-15, 47]. Analogue as well as binary images (with pore space as phase of interest) of specimen sections can be subjected to quantitative analysis. The pore areas observed on section images are defined as pore features. Stereological theory allows straight-forward measurement of volume fraction of

pore space, *i.e.* porosity (p) from section images since area fraction of pore features (*i.e.* area porosity) is an unbiased estimator of porosity, *i.e.* $V_V = \bar{A}_A$ [6, 15, 47]. The bar on top of the parameter indicates an averaging procedure. The stereological notation V_V equals the ratio V_o / V_t, in which V_o and V_t define the observed volume (of the spatial structure) and the total volume, respectively. Similarly, $A_A = A_o / A_t$ with A_o and A_t as the observed area and the total area, respectively. This stereological notation is also used in what follows. Due to the finite resolution of images, the apparent porosity is slightly smaller than the total porosity because pores smaller than the resolution limit cannot be detected.

The perimeter length of 2D pore features per unit test area (L_A in μm^{-1}) can be assigned 3D stereological character via the relationship $S_V = 4\bar{L}_A / \pi$ [6, 47], where S_V is the surface area of pore space per unit test volume (expressed in μm^{-1}). Solid phase is complementary to pore space in section images of cement pastes. Therefore, stereological measurements of average size and spacing of solid phase provide information on pore spacing and pore size, respectively. Mean free spacing between solid phase clusters (defined as average of uninterrupted distance between solid clusters, denoted as λ in (μm), reflects the spatial dispersion of solid phase. It can be adopted therefore as a direct representation of *average pore size*. Similarly, mean intercept length of solid phase clusters ($\bar{L}_3$ in μm) indicates the average pore spacing. According to stereological theory [6], mean free spacing is associated with the volume and surface area of pore space, resulting in $\lambda = 4p / S_V$. Hence, $\bar{L}_3$ can be expressed in porosity and specific surface area by $\bar{L}_3 = 4(1-p) / S_V$. The porosity, specific surface area, average pore size and average pore spacing represent basic characteristics of pore structure. For a more detailed description, see [47].

3.2 ***Morphological opening technique***

Opening is a succession of equally large erosion (*i.e.*, pore features in digitized image are eroded, thereby reducing the relevant area) and dilation operations (*i.e.*, increasing pore area) with an element of a defined size and shape (Fig. 2). All parts of pore structure in 2D, or in 3D alike, that do not re-appear after an opening operation are obviously smaller than the applied element. The area fraction equals the volume fraction in 3D [6, 47]. By stepwise increasing the size of this element, more and more of the 2D pore pattern in the image plane or in the 3D pore structure will disappear, revealing a size smaller than the element of growing size. This way a volume-based pore size distribution is obtained [7, 49, 57, 58].

Obviously, size is defined by the size and shape of the element (*e.g.*, a square). For an application, see [57, 58], also involving obtained data in the form of figures.

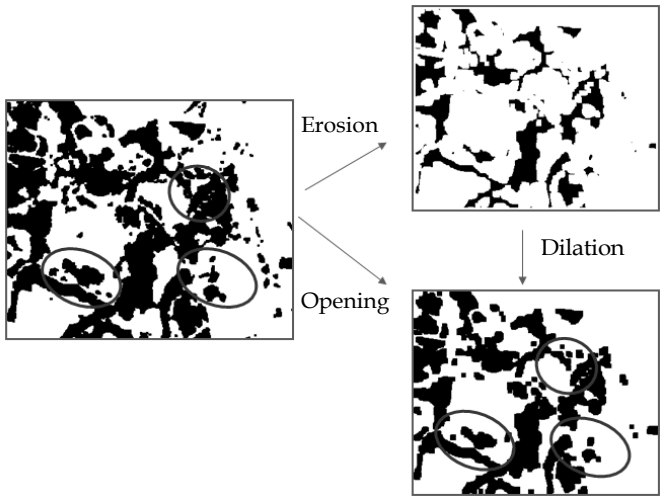

Figure 2. Illustration of an opening operation applied to a digitized image at the left, i.e., an erosion operation followed by a dilation operation with the same structuring element. Please note the structural changes in the indicated regions after application of the opening operation.

3.3 ***Star volume approach***

The main topic targeted in this paper, *star volume measuring* (SVM) is conducted in random points dispersed in 2D of which those outside pore space are neglected. From a specific random point in a pore straight lines are drawn to the nearest pore's perimeter. A large number of such pikes are constructed and their length, l_i , is measured (Fig. 3). SVM says that local pore volume in 3D, V_{p3} , is obtained from measurements of the star pikes l_i that shoot in uniformly random (UR) directions in 2D. Specifically, cubed values of pike lengths are averaged per point, whereupon by the relationship [43, 59]

$$V_{p3} = \frac{\pi}{3}\overline{l_i}^3 \tag{2}$$

the star volume is estimated in 3D. Averaging over a large number of such volumes provides a measure for average pore volume in 3D.

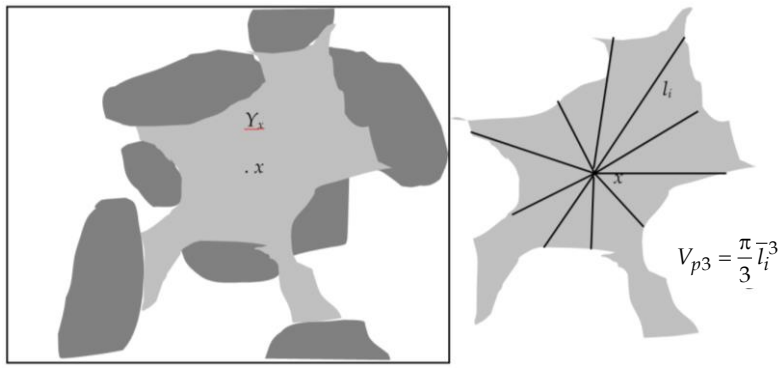

Figure 3. SVM measurements in 2D to estimate pore volume in 3D. (left): Part of schematized field image in which connected pore area (Y_x) in light grey can be observed from random point x. (right): Random point x is the nucleus of a 2D star with pikes in UR directions.

This non-traditional image analysis approach is the starting point for further developments that should lead to the probing pores by stars method for *virtual cementitious materials*. The correct 3D procedure that should be followed and the associated reliability that is achieved are revealed by the proof presented hereafter. Of course, traditional image analysis methods could be applied for obtaining a 2D pore size distribution on the basis of the section image [6]. As stipulated earlier, no simple transfer from 2D to 3D is possible and pore size distribution curves will be fundamentally different as indicated before.

The proof underlying probing pores by stars is based on the following equation

$$V_{p3} = \frac{4\pi}{3}\bar{l}_i^3 \tag{3}$$

leading to a local measure for pore size s

$$s = 2\sqrt[3]{\bar{l}_i^3} \tag{4}$$

for determination of local pore volume in 3D. To prove eq. (3) as basis for 3D probing by stars, consider an arbitrary body configured by a spherical coordinate system (ϕ , θ , r) with bounds $\phi = [\,0, \pi\,]$, $\theta = [\,0, 2\pi\,]$ and $r = [\,0, L(\phi, \theta)]$, where $L(\phi, \theta)$ is a function defining the bounding surface of the body. We have for the infinitely small volume element, dV, depicted by Figure 4,

$$dV = (r\,d\phi)(r\sin\phi\,d\theta)dr = (\sin\phi\,d\phi\,d\theta)r^2 dr \tag{5}$$

The term between brackets in eq. (5) at the right is a constant, *C*, since it represents the infinitely small surface element of a unit sphere.

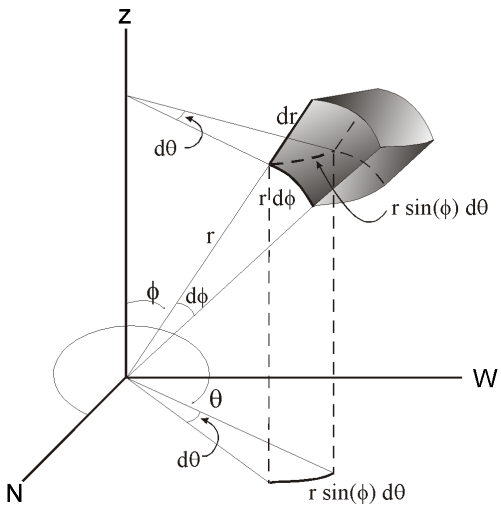

Figure 4. Application of probing pores by stars. Specifically to (pore) surface in 3D.

Next, the volume of the body, *V*, is discretized by tessellation into *n* parts, yielding

$$V \approx \sum_{i=1}^{n} V_i = K\sum_{i=1}^{n}\int_0^{l_i} r^2 dr = K\sum_{i=1}^{n}\tfrac{1}{3}l_i^3 \tag{6}$$

where $l_i = L(\phi_i, \theta_i)$. Further, we have

$$K = \frac{4\pi}{n} \tag{7}$$

Substitution of eq. (7) in (6) yields

$$V \approx \frac{4\pi}{3}\sum_{i=1}^{n}\frac{l_i^3}{n} = \frac{4\pi}{3}\overline{l_i}^3 \;\; (q.e.d.) \tag{8}$$

So, eq. (3) is proven correct. Of course, instead of the tessellation, the surface can also be discretized by a system of uniformly random points distributed on the surface.

2D probing by stars is conducted on the basis of the equivalent expression

$$A = \pi \bar{l}_i^2 \tag{9}$$

The proof is even simpler as compared to that of the 3D case.

4 Porosimetry on compucrete

4.1 Cement particle packing and hydration

At the starting point of the multi-module methodology, the DEM system HADES uniformly random disperses the required number of Portland cement (or other) particles with a designed particle size distribution (generally of Rosin-Rammler type) in a large container. The container has periodic boundaries when bulk material between more remote aggregate particles is simulated. Alternatively, two opposite sides are made rigid and the rest periodic when the cement pocket is supposed situated between nearby aggregate grains. A dynamic stage causes the particles to move and rotate while the container size is gradually reduced (Fig. 5) [51, 55, 60-63]. The HADES system is therefore attributed in the international literature as "dynamic DEM" to distinguish it from "static DEM". HADES represents the most advanced way of simulating particle packing in virtual reality, particularly with the densities met in concrete technology.

Particles could be given non-spherical shape [51, 64, 65] to find a better resemblance to experimental findings such as by Garboczi and Bullard [66] for cement paste and Erdogan *et al*. [67] for aggregate. So far, cement particles were assumed spherical, however, because complicated interference problems will arise during the hydration simulation stage. When two particles encounter each other, leading to some overlap in thin surface layers, the involved elements of the tessellated surface layer cause reactive forces according to designed algorithms. This will lead to re-separation of the particles that thereupon continue to move and rotate. Similar algorithms prevent overlap at the rigid container sides.

When the designed volume density is obtained, or the maximum packing density is arrived at, the procedure stops: the virtual fresh cement paste is available for further study. Figure 5 visualizes the two extreme situations.

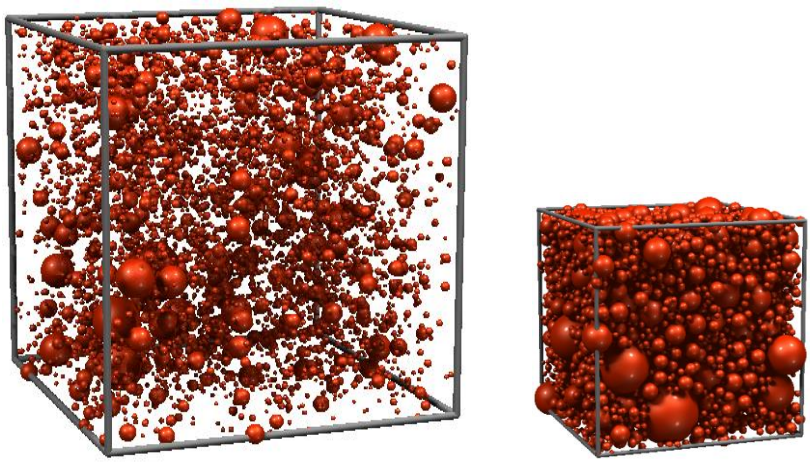

Figure 5. Process of packing simulation by dynamic DEM (HADES). (left): multi-size spherical cement particles in cubic container with periodic boundaries. (right): mixture after dynamic packing to the desired density (after some scale modifications for convenience reasons).

Finally, the capillary pore network develops during hydration simulation of the major compounds of the cement paste by XIPKM [67]. The resulting porous material is thereupon available for porosimetry operations by DRaMuTS at any stage of hydration (Fig. 6).

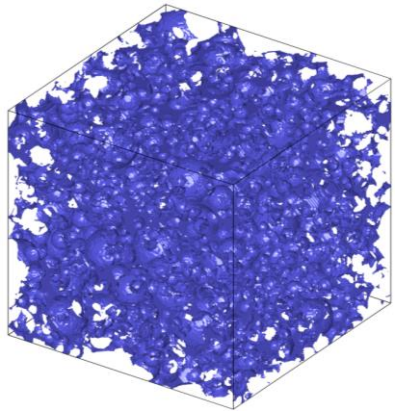

Figure 6. Example of 3D pore network structure that was visualized in the virtual cementitious material after removal of the solid products. This reveals the chaotic and complex character of the pore structure that will be subject of the developed star probing method presented in this paper [55].

4.2 *Pore topology assessment by DRaMuTS*

DRaMuTS operates with improved rapidly-exploring random tree (RRT) algorithms, related to the random walk concept [45, 46]. To that end, a large number of points are UR dispersed in the virtual specimen. Only those inside pore space are considered. The structuring idea is that starting from a point a straight line can be drawn to the neighbouring point without obstruction by a pore surface. If not, a new point is selected closer by the starting point on the unobstructed part of the line. The selection of the new point will violate the UR state of the points of the developing tree-like structures of short straight lines connected in points or nodes and situated fully inside pore space. This process starts in a large number of points. Ultimately, resulting trees may merge because of involving similar parts of pore space. Increasing the number of points will cause smaller and smaller pores to be detected. As a result, the degree of percolation steadily increases to almost one (fully percolated pore structure).

At appropriate sensitivity level, whereby the smaller capillary pores will be excluded (irrelevant in a transport system), a partly de-percolated pore network is depicted by internal zigzag lines of the tree branches (Fig. 7). Topological characteristics of the capillary

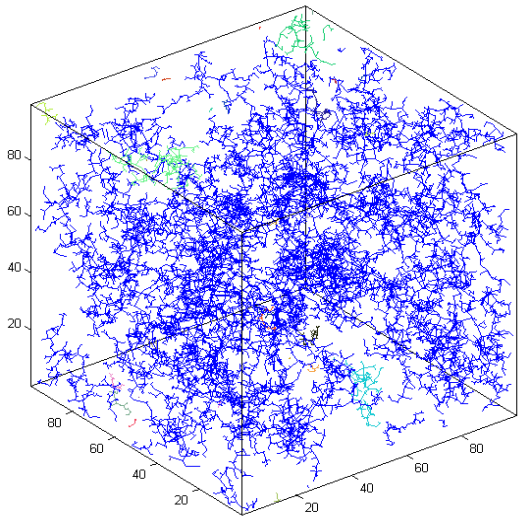

Figure 7. Exploration by the DRaMuTS pore tree system in virtual hydrated blended cement paste with w/b = 0.2 at hydration time of 1440 hours (2 months); fresh cement paste was simulated by DEM (HADES) and casted in 100 µm cubes with two rigid (left and right) and four periodic surfaces. The picture represents an intermediate sensitivity situation at 10,000 tree edges. In light blue, isolated pores that are later removed from the system.

pore network structure can be investigated this way. So, continues pores ("channels") and dead end pores branching of such channels (hence, still belonging to the percolated system because of providing access to both external parallel surfaces of the specimen) and the isolated dead-end pores can be separated from each other. An alternative to assessment of such topological features would be by the extremely cumbersome serial sectioning and 3D reconstruction technique. It was developed in concrete technology for application to virtual cement paste simulated by random sequential simulation by Ye *et al.* [40], and later applied to DEM-produced cement paste by Chen *et al.* [25].

The trees reveal the internal pore network structure, as depicted by Figure 7. For quantification of geometric properties, a second system of UR points is generated (Fig. 8). The point fraction in the pores equals total volume fraction of pores or porosity p.

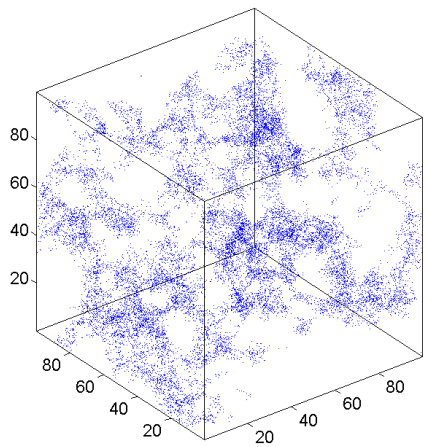

Figure 8. UR dispersed points that are found located inside pore space of the hydrated Portland cement paste of Figure 7. These points constitute the nuclei or nodes for the star probing operation.

Percolated porosity equals therefore the summed up point fractions in channels and in pores branching off these channels. For transport models, the latter fraction would be of low significance and can easily be subtracted for this purpose. Pore tortuosity in the network structure should be obtained as the ratio of continuous pore length and projected length perpendicular to the free surface. The trees can be used for this purpose after applying a smoothening operation to the zigzag lines of the trees. Pore tortuosity is a relevant geometric property in a transport-based model. What is missing is insight into pore size and pore size distribution.

4.3 ***Probing pores by stars***

The developed module for probing pores by stars involves making measurements in all points inside pore space dispersed in the virtual material, and depicted in Figure 8. This renders possible determination of local pore volume and pore size as we will see later (Fig. 9). As an optimum solution for sensitivity, 2×10^5 points are generally dispersed in 100 µm cube space. This offers reliable information on the more sensitive parameters, and still guarantees the economy of the approach.

To estimate permeability by pore network analysis, pore throat, i.e. the smallest local 2D section of a pore, is assessed. Hence this is different from the earlier described concept of the pore tree structure transformed into a compilation of all representative spheres that coalesce to form throats. Along the main route to permeability assessment, the *smallest local pore sections* (throats) per point are determined by 2D probing pores by stars (Fig. 9: left). This requires assessment of the smallest pore area from an isotropic uniformly random (IUR) set of 2D pore sections. Per point, the star's pikes are measured, squared and averaged. Eq. (9) provided a measure for the local pore section area. The root of this value is a 2D measure for pore size and thus for the radius of the representative circle (Fig. 9: right).

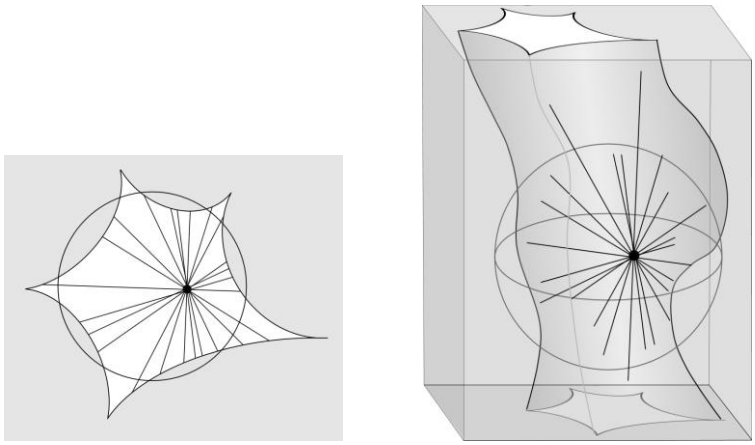

Figure 9 (left): Star probing in 2D for the assessment of the size of the representative circle of the pore section. Random points serve as nuclei for the 2D stars. (right): Star probing in 3D for the assessment of the size of the local representative sphere of the pore. Random points serve as nuclei for the respective 3D stars.

The respective size distribution functions, PoSD (for 3D pore size distribution function; Fig. 9: right) and ToSD (for 2D throat size distribution function; Fig. 9: left), cannot be correlated, as demonstrated by the example of Figure 10 [56]. Yet, determination of the latter one is far more cumbersome and thus time consuming. Still, for prediction of cement permeability, this is considered the more relevant geometric pore network property.

The basic 3D star probing approach is applied to about 2×10^5 points for the determination of PoSD, as stated earlier. However, for the ToSD function, an additional IUR set of 100 to 200 sections is probed by 2D stars. Fortunately, a short method could be developed, based on an old Cauchy theorem [56, 69, 70]. Figure 11 depicts the conceptual set up.

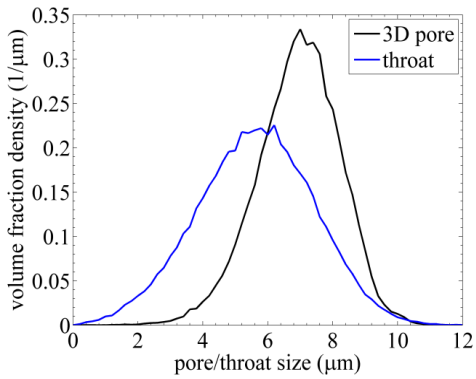

Figure 10. Pore size distribution in 3D (PoSD) and pore throat size distribution in 2D (ToSD) pertaining to the same virtual cement sample (w/c=0.40; Blaine fineness 300 m²/kg). As stipulated earlier, no easy way to correlate both.

Instead of finding in each point of the "random" set the smallest section among the IUR set of star-probed ones, a single "random" section is star-probed (red in Figure 11). The associated representative circles in the 2×10^5 points lead to an area-based (2D) random pore section distribution function (SoSD) that is directly correlated to the ToSD. Specifically, the median 2D pore sizes in the two distributions differ by a factor $\sqrt{2}$. According to Cauchy, the area of a curved surface S in 3D space (in the present case flat; A_i in Figure 11) is given by

$$A' = S\frac{\int_0^{\pi/2}\sin\theta\cos\theta\,d\theta}{\int_0^{\pi/2}\sin\theta\,d\theta} = \frac{1}{2}S \tag{10}$$

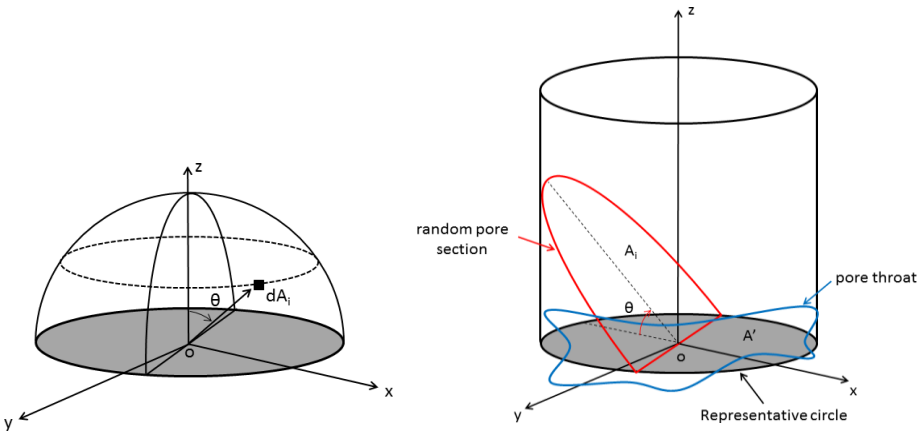

Figure 11. Schematized situation at a throat section in the pore microstructure. The throat is represented by its representative circle of size d and the local pore by a cylinder of equal width. A single randomly oriented pore section from the short approach pertaining to the same throat size is indicated (right). Infinitely small random pore section elements of all random sections pertaining to the same throat size are collected on the surface of the unit sphere (left).

Hence the average projected area of the random pore sections of equal throat size A' on this throat section is twice as large as A'. Since this equally holds for each pore throat size, it is valid for the complete range of pore throat sizes. So, with 2 as area ratio, we have $\sqrt{2}$ for the size ratio. In [56] this result was validated on the basis of a large number of investigated cement mixtures. The number of projections in the Cauchy approach has been proven relatively small to arrive at a desired level of reliability [53, 54]. This would imply that in the future, one could eventually further reduce the efforts of 2D star probing in random sections of a smaller population than provided for by the 2×10^5 dispersed points.

Porosimetry as well as permeability estimation is accomplished by successive operation, embodied by modules. DEM particle packing, XIPKM hydration simulation, DRaMuTS pore delineation, star probing and eventually network analysis require all about one hour for completion. The time required for probing by stars can be reduced by 85% when the indicated "Cauchy route" is followed. This has one serious drawback, however. The size information obtained cannot be used as input in the pore network module, since the information is of global nature. Hence, a globalized estimation procedure for permeability should be pursued, whereby additional information on *tortuosity* is obtained in the

DRaMuTS module and shape is accounted for by a linear relationship between a shape factor (versus that of a circle) and conductivity (versus that of a circular cross section) obtained by FET approach for a couple of hundred throat sections. This way of accounting for the effect of irregular shape of pore sections on transport capability of the pore network system is also successfully employed in the standard 3D network approach.

5 Discussion and conclusions

SVM applied for porosimetry in experimental settings is fairly unknown in concrete technology. For virtual cementitious materials (primarily blended cement pastes) this concept has been elaborated further for the development of probing pores by stars, in accordance with our formulated research goal. Result should be estimating pore size (as the diameter of the representative sphere) by 3D stars situated inside pore space. The way how to realize this was also part of the research goal and was discussed in the foregoing. Since, we followed the analogue route to avoid the well-known shortcomings of a digitized materials concept, the morphological opening technique could not be considered. Moreover, dispersed elements are more appropriate for analysis by the morphological opening technique. Finally, obtained size should be locally linked to the tree-like structure, which is not possible with the opening technique.

SVM as non-traditional stereological technique is applied basically in 2D in experimental set ups, however with the inherent capability to estimate 3D size, as indicated herein. In the virtual approach, both 3D as well as 2D probing by stars can be accomplished. The reliability of both approaches was proven guaranteed. The 3D approach provides the proper information on the complex spatial *geometry* of the pore structure in the material. Alternatively, the 2D star probing approach yields the required input information for a classical pore network analysis to estimate *permeability* of the compucrete (*i.e.*, virtual cement paste). Efforts bestowed on this stage can be significantly reduced by making use of a Cauchy theorem (hence, stereology *avant la letter*), as demonstrated herein, and depicted by Figure 11. The resulting globalized methodology for permeability assessment can further be completed with tortuosity information obtained by DRaMuTS. Finally, pore shape effects on conductivity are accounted for in the different permeability estimation concepts by a linear relationship obtained by FET on a couple of hundred sections.

Although not directly of concern with respect to pore probing by stars, it should nevertheless be mentioned that the data obtained deal with the cement paste pocketed between the dispersed aggregate grains in the concrete. For *concrete* based on crushed rock or river gravel aggregate, the permeability of the concrete can be derived simply from that of the cement paste by accounting for the dilution and the tortuosity effects of the aggregate [71, 72], which may cause a permeability decline of roughly one order of magnitude.

Nevertheless, a gap seems to exist between experimentally obtained (water) permeability and predictions based on the discussed methodology. However, most of the experimental data are based on MIP that has been proven leading to seriously biased (i.e., too small) pore size information [1, 2]. See also Figure 12, which indeed reveal the significant gap with the quantitative image analysis results.

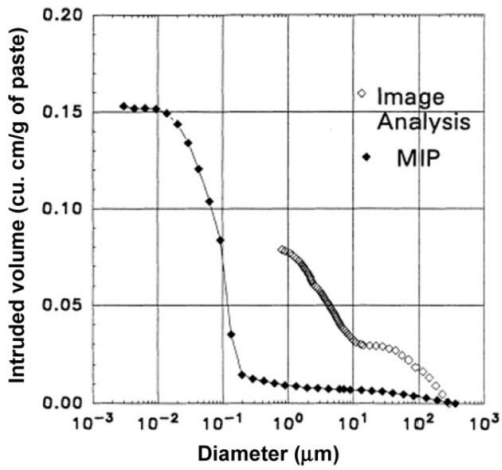

Figure 12. Huge differences between porosimetry results obtained by quantitative image analysis and by MIP assessed on similar cementitious material samples [1]

Further, the used specimens are assumed fully water saturated. This has been shown not representing the actual situation [61, 72-77]. The inevitable reduced water saturation degree in the investigated specimens will thus further (significantly) reduce the permeability data, as shown in Figure 13. Hence, the suggested gap between experimental outcomes and estimated results based on the presented virtual approach are probably small. Finally, advanced research has shown the outer hydration layer of cement paste also

of particulate nature and not of uniform density, as assumed in the XIPKM approach. Yet, in this case on nano-level [78].

Virtual approaches using the principles outlined in this paper, indeed demonstrate that pore size will thereby be reduced and the surface of the pore roughened [28, 71, 76], as depicted by the 2D illustrative example of Figure 14. The latter is particularly ignored in the vector-based XIPKM approach. All in all, this may provide the last relatively small step to get *proper* experimental data on permeability from realcrete and similar estimates for compucrete to match. This should ultimately be the stimulus for using the far more economical approach focusing on compucrete, of which the module "probing pores by stars" forms a crucial part.

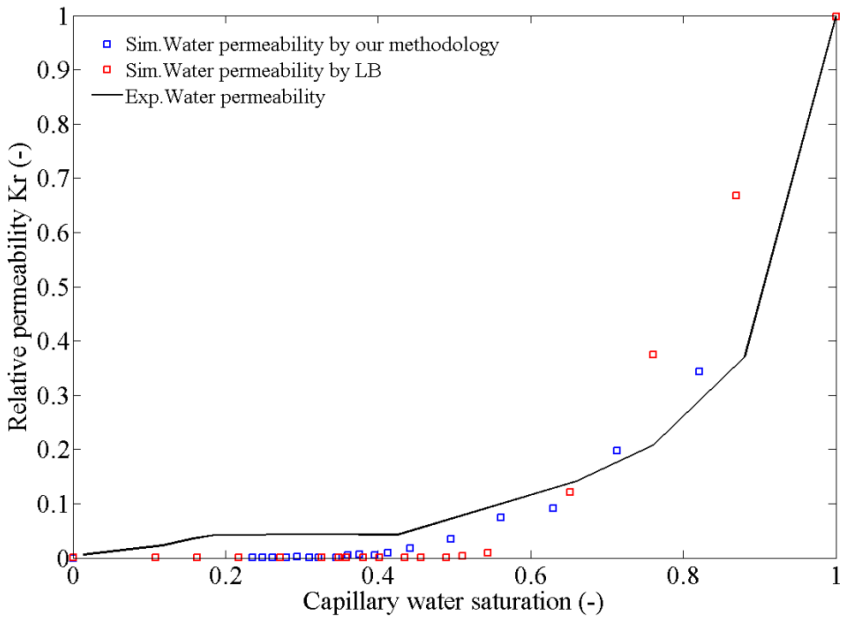

Figure 13. Effect of stagnant water content in pore system in virtual DEM-based hydrated cement paste on relative permeability Kr. Experimental data for hardened concrete with various amounts of stagnant water in the pore system are from (Kameche, et al. [79]). LB represents Lattice Boltzmann method used for permeability calculation in RSA-based structure in (Zalzale, et al. [80]). DEM data are much closer to experimental ones than those of RSA.

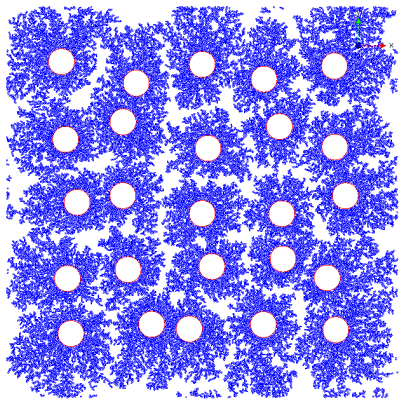

Figure 14. 2D simulation, for illustrative purposes only, of an intermediate hydration stage of fibrous C-S-H in the outer hydration layer consisting of aggregated 50 nm nodules around 25 µm cement grains (+ inner hydration layer). Smaller and surface roughened pores are resulting in comparison with the XIPKM approach [71, 76].

References

[1] Diamond, S. (2000). Mercury porosimetry; an inappropriate method for the measurement of pore size distributions in cement-based materials. *Cem. Concr. Res*.. 30 (10): 1517-25.

[2] Willis, K.L., Abell, A.B., Lange, D.A. (1998). Image-based characterization of cement pore structure using Wood's metal intrusion. *Cem. Concr. Res*., 28(12): 1695-705.

[3] Stroeven, P., Hu, J., Stroeven, M. (2009). On the usefulness of discrete element computer modeling of particle packing for material characterization in concrete technology. *Comp. Concr*., 6(2): 133-153

[4] Williams, S.R., Philipse, A,P. (2003). Random packings of spheres and spherocylinders simulated by mechanical con traction. *Phys. Rev*. E; 67(051301): 1-9.

[5] Li, K., Stroeven, P. (2018). RSA vs DEM in view of particle packing-related properties of cementitious materials. *Comp. Concr*. 22(1):83-91

[6] Underwood, E.E. (1968). *Quantitative Stereology*, Addison-Wesley Publ.

[7] Hu, J. (2004). *Porosity of concrete; morphological study of model concrete*. PhD Thesis, Delft Univ. Techn., OPTIMA, Delft. The Netherlands.

[8] Wong, H.S., Buenfeld, N.R., Head, M.K. (2006). Estimating transport properties of mortars using image analysis on backscattered electron images. *Cem. Concr. Res*., 36(8):1556-1566.

[9] Scrivener, K.L. (1989). The use of backscattered electron microscopy and image analysis to study the porosity of cement paste., In: *Proc. Material Research Society Symposium 137*, (Roberts, LR., Skalny, J.P. Eds.), Boston, pp. 129-140.

[10] Roels, S., Elsen, J., Carmeliet, J., Hens, H. (2001). Characterization of pore structure by combining mercury porosimetry and micrography. *Mat. Struct*., 34(2): 76-82.

[11] Lange, D.A., Jennings, H.M., Shah, S.P. (1994). Image analysis techniques for characterization of pore structure of cement-based materials. *Cem. Concr. Res*. 24(5): 841-853.

[12] Wang, Y., Diamond, S. (1995). An approach to quantitative image analysis for cement pastes. In: *Proc. Mat. Res. Soc. 370*, (Diamond S, Mindess S, Glasser FP, Roberts LW, Skalny JP, Wakeley LD Eds.), Pittsburgh, pp. 23-32

[13] Stroeven, P., Hu, J., Guo, Z. (2009). Shape assessment of particles in concrete technology - 2D image analysis and 3D stereological extrapolation, *Cem.Concr. Comp*. 31: 84–91.

[14] Hu, J., Stroeven, P. (2003). Application of image analysis to assessing critical pore size for permeability prediction on cement paste. *Im. Anal. Stereol*., 22(2):97-103.

[15] Serra, J. (1982) *Image Analysis and Mathematical Morphology*, Academic Press, London.

[16] Diekämper, R. (1984). *Ein Verfahren zur numerischen Simulation des Bruch- und Verformungsverhaltens spröder Werkstoffe*, Technische Wissenschaft-liche Mitteilungen der Institut für Konstruktiven Ingenieursbau, Ruhr Universität Bochum.

[17] Breugel, K. van (1991). *Simulation of hydration and formation of structure in hardening cement-based materials*. PhD Thesis Delft Univ. Techn., DUP, Delft, the Netherlands..

[18] Bentz, D.P., Garboczi, E.J., Stutzman, P.E. (1993). Computer modeling of the interfacial transition zone in concrete. In: *Interfaces in Cementitious Compo-sites*, E&FN Spon, London, pp. 107-116

[19] Meakawa, K., Chaube, R., Kishi, T. (1999). *Modeling of concrete performance -hydration, micro-structure formation and mass transport*, E&FN Spon, London.

[20] Xu, W.H., Chen, H.S., (2012). Micro-structural characterization of fresh cement paste via random packing of ellipsoidal cement particles. *Mat. Charact*. 66:16-23

[21] Bishnoi S., Scrivener K.L. (2009). µic: A new platform for modelling the hydration of cements. *Cem. Concr. Res*. 39(4):266-274.

[22] Roelfstra, P.E. (1989). *A numerical approach to investigate the properties of numerical concrete*. PhD Thesis, Ecole Polytechnique Fédérale de Lausanne, Lausanne, Switzerland

[23] Stroeven, P., Hu, J., Chen, H. (2008). Stochastic heterogeneity as funda-mental basis for the design and evaluation of experiments. *Cem. Concr. Comp*. 30:506-514,

[24] Freudenthal, A.M. (1950). *The inelastic behaviour of engineering materials and structures*. Wiley, New York.

[25] Chen, H., Stroeven, P., Ye, G., Stroeven, M. (2006). Influence of boundary conditions on pore percolation in model cement paste. *Key Engrn. Mat*. 302-303:486-492

[26] Garboczi, E.J., Bentz, D.P. (2001). The effect of statistical fluctuation, finite size error, and digital resolution on the phase percolation and transport properties of the NIST cement hydration model. *Cem Concr Res*. 31:1501-14.

[27] Stroeven, P., Hu, J. (2008). Stochastic heterogeneity as fundamental basis for the design and evaluation of experiments, *Cem. Concr. Comp*. 30:605-610.

[28] Stroeven, P., Li, K., Le, L.B.N., He, H., Stroeven, M. (2015). Capabilities for property assessment on different levels of the microstructure of DEM-simulated cementitious materials. *Constr. Build. Mat*. 88:105-117

[29] Mościński, J., Bargieł, M., Rycerz, Z.A., Jacobs, P.W.M. (1989). The force-based algorithm for irregular close packing of equal spheres. *Mol. Simul*. 3:201-212.

[30] Markausas, D., Kačianauskas, R. (2006). Compacting of particles for biaxial compression test by discrete element method. *J. Civ. Engrg. Manag*. XII(2): 153-161.

[31] Tsunekawa, H., Iwashita, K. (2001). Numerical simulation of triaxial test using two and three dimensional DEM. In: *Proc. 4th Int. Conf. Micromechanics of granular media, powder and grains*. Balkema, Rotterdam, pp. 177-180.

[32] O'Connor, R.M., Troczynski, J.R., Klosek, J.T., Williams, J.R. (1997). Discrete element modelling of sand production. *Int. J. Rock. Mech. Mining Sc.* 34(3-4) paper 231.

[33] Jodrey, W.S., Torey, E.M. (1981). Computer simulation of isotropic, homogeneous, dense random packing of equal spheres. *J. Powd. Techn*., 30:111-118.

[34] Ansell, G.C., Dickinson, E. (1986). Sediment formation by Brownian dynamics simulation: effect of colloidal and hydrodynamic interaction on the sediment structure. *J. Chem. Phys*. 85(7): 4079-4086.

[35] Li, J-F., Yu, W-H., Chen, C-S., Yu, B-Y., Wei, W-C. (2006). Simulation of colloidal particle packing for photonic bandcap crystals. *J. Am. Ceram. Soc*. 89(4):1257-1265.

[36] Klosek, J.T. (1997). *The integration of fluid dynamics with discrete-element modeling systems: algorithms, implementations and applications*. MSc Thesis MIT, Dept. Civil and Environmental Engineering, Boston.

[37] Puri, U.C., Uomoto, T. (2002). Characterization of distinct element modeling parameters for fresh concrete and its application in shotcrete simulations. *J. Mat. Civ. Eng*. 14(2):137-144.

[38] Mechtcherine, V., Gram, A., Krenzer, K., Schwabe, J.H., Shyshko, S., Roussel, N. (20014). Simulating the behaviour of fresh cement with the discrete element method – Deriving model parameters related to the yield stress. *Mat. Struct.* 47:615-630

[39] O'Connor, R.M. (1996). *A distributed discrete element modelling environment – Algorithms, implementations and applications*. PhD. Thesis, M.I.T., Boston.

[40] Ye, G., Hu, J., van Breugel, K., Stroeven, P. (2002). Character-ization of the development of microstructure and porosity of cement-based materials by numerical simulation and ESEM image analysis. *Mat. Struct*., 35:603-613.

[41] Ikuta, A., Kumasaka, S., Kashima, I. (2000). Quantitative analysis using star volume method applied to skeletton patterns extracted with a morphological filter. *J. Bone Miner. Metabol*., 19(5):271-277

[42] Higgins, M.D. (2006). *Quantitative textural measurements in igneous and metamorphic petrology*. Cambridge Univ. Press

[43] Gundersen, H.J.G., et al. (1988). Some new stereological tools - and their use in pathological research and diagnosis. *Acta Pathol. Microbiol. Immun. Scand.*, 96:379-394 and 857-881

[44] Stroeven, P., Le, L.B.N., Sluys, L.J., He, H. (2012). Porosimetry by double random multiple tree structuring. *Im. Anal. Stereol.*, 31:55-63

[45] LaValle, S.M., Kuffner, J.J. (2001). Rapidly exploring random trees – Progress and prospects. In: *Algorithmic and Computational Robotics: New Directions*, (B. R. Donald, K. M. Lynch, and D. Rus, Eds.). A K Peters, Wellesley (MA). pp. 293-308.

[46] LaValle, S.M., Kuffner, J.J. (2001). Randomized kinodynamic planning. *Int. J. Robotics Res.*, 20(5):378-400

[47] Stroeven, P., Hu, J. (2006). Review paper: Stereology - Historical perspective and applicability to concrete structures. *Mat. Struct.*, 39:127-135

[48] Stroeven, P. (2015). *50 Years' focus on concrete - from meter- to nano-scale 1963-2013*. MediaCenter, Rotterdam.

[49] Hu, J., Stroeven, P. (2004). Size characterization of pore structure for estimating transport properties of cement paste. In: *Proc. Int. Conf. Computational and Experimental Engineering and Sciences* (ISBN: 0-9657001-6-X), paper ID 146, Portugal, available on proc. CD.

[50] Delfiner P. A. (1971). Generalization of the concept of size. *J. Microsc.* 95:203-216

[51] He, H. (2010). *Computational Modelling of Particle Packing in Concrete*, PhD Thesis, Delft Univ. Techn., Delft, the Netherlands.

[52] Vieser, W. (1926). Proportioning concrete, *Zement*, Sept/Oct.

[53] Stroeven, P. (1973). *Some aspects of the micromechanics of concrete*, PhD Thesis Delft Univ. Techn. DUP, Delft.

[54] Kendall, M.G., Moran, P.A.P. (1963). *Geometric probability*, Butler & Tanner Ltd, London

[55] Stroeven, M. (1999). *Discrete numerical modelling of composite materials – application to cementitious materials*, PhD Thesis Delft Univ. Techn., Meinema, Delft, the Netherlands.

[56] Stroeven, P., Li, K. (2017). A modern approach to porosimetry of virtual cementitious materials. *Mag. Concr. Res.* 69(23):1212-1217

[57] Stroeven, P., Hu, J., Koleva D.A. (2010). Concrete porosimetry: aspects of feasibility, reliability and economy, *Cem. Concr. Comp.* 32(4):291-299.

[58] Hu, J., Stroeven, P. (2005). Depercolation threshold of porosity in model cement; approach by morphological evolution during hydration. *Cem. Concr Comp.* 27(1):19-25.

[59] Gundersen, H.J.G., Jensen, E.B. (1985). Stereological estimation of the volume-weighted mean volume of arbitrary particles observed on random sections. *J. Microsc.* 138:127-142.

[60] Le, L. B. N. (2015). *Micro-level porosimetry of virtual cementitious materials – Structural impact on permeability on unsaturated cementitious materials*. PhD Thesis Delft Univ. Techn., Delft, the Netherlands.

[61] Li, K. (2017). *Numerical determination of mechanical and durability evolution*, PhD Thesis, Delft Univ. Techn., Delft, the Netherlands

[62] Stroeven, P., Guo, Z. (2006). Modern routes to explore concrete's complex pore space. *Im. Anal. Stereol.* 25:75-86

[63] Stroeven, P., Hu, J., Stroeven, M. (2009). On the usefulness of discrete element modeling of particle packing for material characterization in concrete technology. *Comp. Concr.*, 6:133-153

[64] He, H., Guo, Z., Stroeven, P., Stroeven, M., Sluys, L.J. (2010). Strategy on simulation of arbitrary-shaped cement grains in concrete. *Im. Anal. Stereol.* 29:79-84

[65] He, H., Stroeven, P. (2012). Particulate structure and meso-structure evolution of concrete investigated by DEM, Part I and II. *HERON*, 57(2):119-132 and 133-150

[66] Garboczi, E.J., Bullard, J.W. (2004). Shape analysis of a reference cement. *Cem. Concr. Res.* 34(10):1933-1937

[67] Erdogan, S.T., Quiroga, P.N., Fowler, D.W., Saleh, H.A., Livingston, R.A., Garboczi, E.J., et al. (2006). Three dimensional shape analysis of coarse aggregate: new techniques for and preliminary results on several different coarse aggregates and reference rocks. *Cem. Concr. Res.* 36:1619-1627.

[68] Le, L.B.N., Stroeven, M., Sluys, L.J., Stroeven, P. (2013). A novel numerical multi-component model for simulating hydration of cement. *Comp. Mater. Sci.* 78:12-21

[69] Li, K., Stroeven, P. (2017). Heron's Fountain 18: 200 years old Cauchy concept pointed the route to optimizing concrete porosimetry in virtual reality. *HERON*, 62(2):119127.

[70] Cauchy, A. (1882). *Mémoires sur la rectification des courbes et la quadrature des surfaces courbes*. Cambridge Univ. Press, Cambridge (UK) (in French).

[71] Li, K., Stroeven, P., Sluys, L.J. Nano-level C-S-H packing simulation can bridge the gap between conventional experimental and numerical approaches to concrete permeability (publication in preparation)

[72] Stroeven, P. (2000). A stereological approach to roughness of fracture surfaces and tortuosity of transport paths in concrete. *Cem. Concr. Comp*. 22:331-341

[73] Kameche, Z.A., Ghomari, F., Choinska, M., Khelidj, A. (2014). Assessment of liquid water and gas permeability of partially saturated ordinary concrete, *Constr. Build. Mater*. 65:551-565

[74] Zalzale, M., McDonnald, P.J., Scrivener K.L. (2013). A 3D lattice Boltzmann effective media study: understanding the role of C-S-H and water saturation on the permeability of cement paste *Modelling Simul. Mater. Sci. Eng*. 21:085016

[75] Zamani, S., Kowalczyk, R.M., McDonald, P.J. (2014). The relative humidity dependence of the permeability of cement paste measured using GARField NMR profiling, *Cem. Concr. Res*. 57:88-94

[76] Li, K., Stroeven, M., Stroeven, P., Sluys, L.J. (2017). Effects of technological parameters on permeability estimation of partially saturated cement paste by a DEM approach. *Cem. Concr. Comp*. 84:222-231.

[77] Li, K., Stroeven, M., Stroeven, P., Sluys, L.J. (2016). Investigation of liquid water and gas permeability of partially saturated cement paste by DEM approach, *Cem. Concr. Res*. 83:104-113.

[78] Jennings, H.M. (2000). A model for the microstructure of calcium silicate hydrate in cement paste. *Cem. Concr. Res*. 30:101-116

[79] Kameche ZA, Ghomari F, Choinska M and Khelidj A (2014) Assessment of liquid water and gas permeabilities of partially saturated ordinary concrete. *Construction and Building Materials* 65: 551-565.

[80] Zalzale, M., McDonnald, P.J, Scrinener, K.L. (2013). A 3D lattice Bolzmann effective media study: understanding the role of C-S-H and water saturation on the permeability of cement paste, *Modelling Simul. Mater. Sci. Eng*., 21:085016